Open-Circuit Fault-Tolerant Control for Outer Switches of Three-Level Rectifiers in Wind Turbine Systems

June-Seok Lee, *Student Member, IEEE*, and Kyo-Beum Lee, *Senior Member, IEEE*

***Abstract*—A three-level converter is used as the power converters of wind turbine systems because of their advantages such as low-current total harmonic distortion, high efficiency, and low collector–emitter voltage. Interior permanent magnet synchronous generators (IPMSGs) have been chosen as the generator in wind turbine systems owing to their advantages of size and efficiency. In wind turbine systems consisting of the three-level converter and the IPMSG, fault-tolerant controls for an open-circuit fault of switches should be implemented to improve reliability. This paper focuses on the open-circuit fault of outer switches (S_{x1} and S_{x4}) in three-level rectifiers (both neutral-point clamped and T-type) that are connected to the IPMSG. In addition, the effects of S_{x1} and S_{x4} open-circuit faults are analyzed, and based on this analysis, a tolerant control is proposed. The proposed tolerant control maintains normal operation with sinusoidal currents under the open-circuit fault of outer switches by adding a compensation value to the reference voltages. The effectiveness and performance of the proposed tolerant control are verified by simulation and experiment.**

***Index Terms*—Neutral-point-clamped rectifier, open-circuit fault, open-switch fault, reliability, three-level topology, tolerant control, T-type rectifier.**

NOMENCLATURE

pf	Power factor.
$I_{\rm rec}$	Rectifier input current.
$I_{x,\rm rec}$	Rectifier input current of *x*-phase.
$V_{\rm rec}$	Rectifier input voltage.
$V_{x,\rm rec}$	Rectifier input voltage of *x*-phase.
$V_{\rm EMF}$	Back EMF of PMSG.
φ_Z	Phase difference (°) between $V_{\rm EMF}$ and $V_{\rm rec}$.
φ_{pf}	Phase difference (°) between $I_{\rm ref}$ and $V_{\rm EMF}$.
$V_{x,\rm ref}$	Reference voltage of *x*-phase.
$V_{\rm mag}$	Magnitude of the reference voltages.
f_s	Fundamental frequency (Hz) represented the angular frequency of the PMSG.
$V_{\rm ref,max}$, $V_{\rm ref,min}$	Maximum and minimum values of $V_{a,\rm ref}$ $V_{b,\rm ref}$, and $V_{c,\rm ref}$.
$V_{\rm comp}$	Compensation voltage of the proposed tolerant control.
R	Equivalent resistance (Ω) of the PMSG.
L	Equivalent inductance (H) of the PMSG.
I_{qe}, I_{de}	*d*-axis and *q*-axis currents in the d–q synchronous rotating frame.
$\theta_{\rm EMF}$	$V_{\rm EMF}$'s angle.
M_a	Modulation index, $\sqrt{3} \times V_{\rm mag}/V_{\rm dc}$.

Manuscript received April 28, 2015; revised June 19, 2015; accepted July 27, 2015. Date of publication August 5, 2015; date of current version December 10, 2015. This work was supported by the Basic Science Research Program through the National Research Foundation of Korea funded by the Ministry of Education (2013R1A1A2A10006090). Recommended for publication by Associate Editor H. Li.

The authors are with the Department of Electrical and Computer Engineering, Ajou University, Suwon 443-749, Korea (e-mail: junpb@ajou.ac.kr; kyl@ajou.ac.kr).

Color versions of one or more of the figures in this paper are available online at http://ieeexplore.ieee.org.

Digital Object Identifier 10.1109/TPEL.2015.2464803

I. INTRODUCTION

THE power capacity of a wind turbine system has been increasing consistently, leading to the development of generators with large power capacity [1]–[3]. There are many types of generators. Permanent magnet synchronous generators (PMSGs) have high efficiency and high reliability compared with induction generators. This is because external excitation is not required and there are no copper losses in the rotor circuits. Moreover, because of the smaller size of the PMSG, the weight of the wind turbine is reduced [4]. Among various PMSGs, interior PMSGs (IPMSGs) are especially advantageous from the standpoints of efficiency and power generation owing to the use of the reluctance torque [4]–[7].

Generators requiring high voltage need to use multilevel converter topologies to reduce the collector–emitter voltage per switch. Among multilevel topologies, three-level topologies such as the three-level neutral-point clamped (3L-NPC) and T-type topologies are applied in wind turbine systems with a wide power range. The three-level topology can easily be expanded from a two-level topology and is also easier to control compared with other multilevel topologies. Furthermore, the three-level topology guarantees high efficiency and low-current total harmonic distortion (THD) in comparison with the two-level topology [8]–[11].

The 3L-NPC topology is vulnerable to switch faults because many switches are used. Switch fault detection and tolerant control methods for switch faults should be implemented to improve the reliability of wind turbine systems. Switch faults are divided into a short-circuit fault and an open-circuit fault [12]. The short-circuit fault normally leads to a breakdown of the entire system; therefore, fault detection and tolerant control methods for the short-circuit fault require additional circuits. On the other hand, the open-circuit fault leads to current distortion, which can lead to a breakdown if it persists for a long time; therefore, the open-circuit fault should be detected, and the tolerant controls are necessary [9], [12]–[15].

In wind turbine systems, a back-to-back converter is used to transfer power from the generator to the grid. A back-to-back converter using the 3L-NPC topology is shown in Fig. 1.

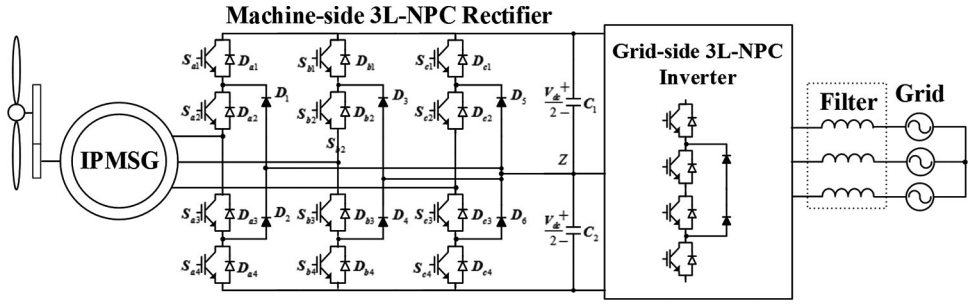

Fig. 1. Back-to-back converter using the 3L-NPC topology in wind turbine systems.

This consists of the machine-side 3L-NPC rectifier, the dc-link, and the grid-side 3L-NPC inverter. Depending on the operating conditions, tolerant controls can be applied for the rectifier or the inverter because the current paths of the rectifier and the inverter are different [9], [13]–[15]. In addition, the different structure of the three-level topologies should be considered in the tolerant controls [9], [13].

In the 3L-NPC inverter, the open-circuit fault of the inner switch causes the outer switch connected it to be infeasible; therefore, changing only the switching method does not become a solution for the open-circuit fault, and the additional devices such as fuses and switches should be added for achieving the tolerant operation under the open-circuit fault of the inner switch [16]–[18]. However, the open-circuit fault of the outer switch can be handled by changed the switching method in limited range [19]. In [19], the tolerant control method limits the output voltage range by half. In the 3L-NPC rectifier, the current distortion caused by the open-circuit fault of the inner switch can be restored partially by clamping the switching state without any additional devices [14]. In addition, the reactive current is injected to eliminate current distortion caused by the open-circuit fault of the outer switch [22]. This method can also be applied for the T-type rectifier. The T-type rectifier is advantageous on the tolerant control because the switches in a leg are independent of each other. Many tolerant control methods for the open-circuit fault of the inner switch, which can be used in both the T-type inverter and rectifier, were proposed in [13], [14], and [20]–[21]. These methods change the switching method to disable the switch with the open-circuit fault and do not need the additional devices.

This paper focuses on the open-circuit fault of the machine-side 3L-NPC rectifier. In general, the input currents of the 3L-NPC rectifier do not flow through the outer switches (S_{x1} and S_{x4}) at unity power factor (*pf*); therefore, the existing tolerant controls for the 3L-NPC rectifier take into account only the inner switches (S_{x2} and S_{x3}) [13]. However, according to the specification of the PMSG, an open-circuit fault of the outer switch can cause current distortion as much as when an open-circuit fault of the inner switch occurs [22]. The tolerant control for S_{x1} and S_{x4} open-circuit faults is also proposed in [22], and this control method injects the exact reactive current required to eliminate the current distortion. This means that the *pf* is changed.

Rectifiers with IPMSGs can operate to generate maximum power at *pfs* other than unity. IPMSGs provide more power when rectifiers operate at a unique *pf* [4]–[7]. In such a case, an open-circuit fault of the outer switches (S_{x1} and S_{x4}) causes current distortion and torque fluctuation, which can lead to vibration of the wind turbine. In this paper, the reason for the current distortion caused by the outer switches (S_{x1} and S_{x4}) is analyzed, and then, on the basis of this analysis, a tolerant control for S_{x1} and S_{x4} open-circuit faults is proposed. In the proposed tolerant control, the switch with an open-circuit fault is not used to generate the input voltages of the three-level rectifier by adding a compensation value to the reference voltages. The compensation value is simply calculated and the *pf* does not change in the proposed tolerant control. The performance of the proposed tolerance control is proved by simulation and experiment.

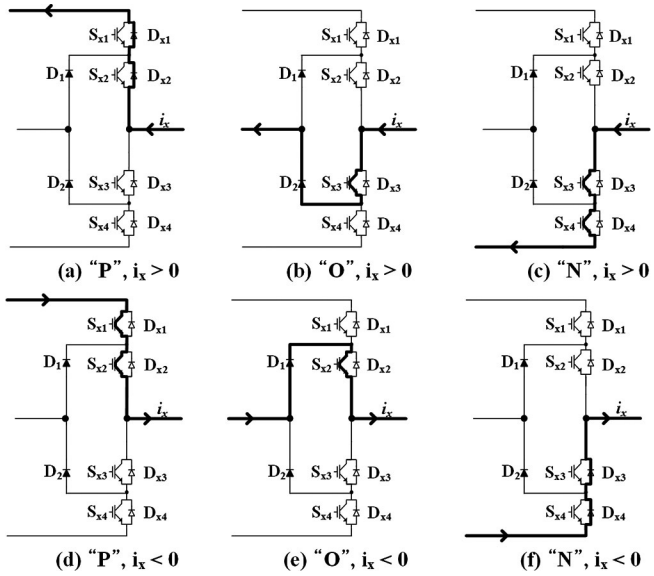

Fig. 2. Current paths depending on the current direction and the switching state.

II. Open-Circuit Fault Analysis of Outer Switches

There are three switching states (P, N, and O) in the 3L-NPC rectifier [9]. Six current paths can be generated depending on the current direction and the switching state, and these are shown in Fig. 2 [23].

Fig. 3 shows the input current generation process of a rectifier with unity *pf*. The rectifier current is $I_{\rm rec}$, the rectifier voltage is $V_{\rm rec}$, and the back electromotive force (EMF) is $V_{\rm EMF}$. The

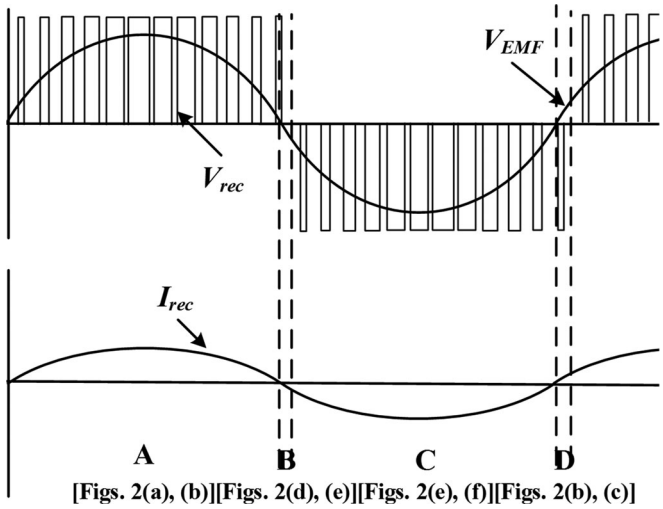

Fig. 3. Rectifier operation at unity *pf*.

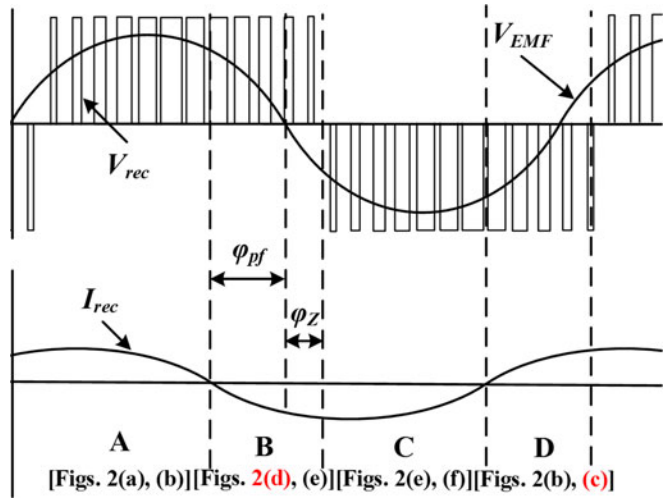

Fig. 4. Rectifier operation at any *pf*.

TABLE I
CURRENT PATH COMPOSITION DEPENDING ON THE PART OF FIG. 3

Part	$V_{\rm rec}$	$I_{\rm rec}$	Current path
A	Positive	Positive	(a) P switching state, (b) O switching state (valid)
B	Positive	Negative	(d) P switching state (valid), (e) O switching state
C	Negative	Negative	(e) O switching state (valid), (f) N switching state
D	Negative	Positive	(b) O switching state, (c) N switching state (valid)

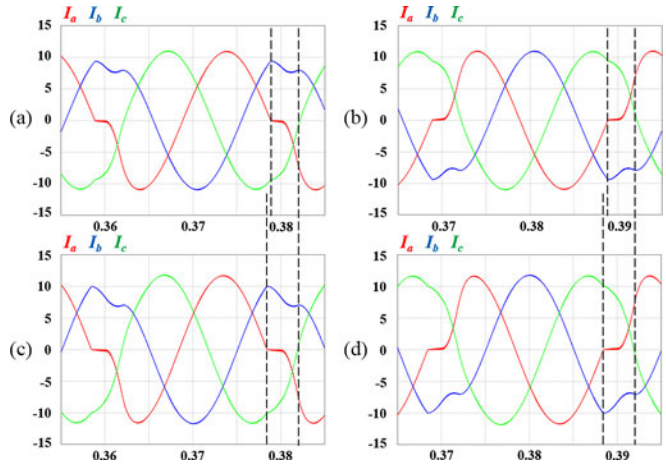

Fig. 5. Current distortion depending on the open-circuit fault and the *pf*: (a) 0.95 *pf*, S_{x1} open-circuit fault, (b) 0.95 *pf*, S_{x4} open-circuit fault, (c) 0.9 *pf*, S_{x1} open-circuit fault, and (d) 0.9 *pf*, S_{x4} open-circuit fault.

phase difference between $V_{\rm EMF}$ and $V_{\rm rec}$, which causes the current flow, is controlled to match the phase of $I_{\rm rec}$ up with the phase of the corresponding $V_{\rm EMF}$. One period of $I_{\rm rec}$ can be divided into four parts depending on the polarity of $I_{\rm rec}$ and $V_{\rm rec}$. The generated current paths are different depending on the part, and these are summarized in Table I. In parts A and C, the O switching state causes the input current flow; therefore, this is called the valid switching state. The current continuously flows through two diodes if the switching state is changed to P or N switching state in which no current flows through the switches. In parts B and D, the P and N switching stages are the valid switching state where the current flows through the switches. When the rectifier operates with unity *pf*, parts A and C are large, and parts B and D are small. If parts B and C are very small as much as be ignored, the S_{x1} and S_{x4} open-circuit faults can be ignored [22], [23].

However, parts B and D can be extended in Case I when $V_{\rm EMF}$ is small and a large $I_{\rm rec}$ is required [22]. This is because the phase difference between $V_{\rm EMF}$ and $V_{\rm rec}$ becomes large. In this paper, the other case (Case II), which is the reactive current injection for IPMSG, is also considered. Fig. 4 shows that the input current generation process of the rectifier for Cases I and II.

There are two phase differences: the phase difference (φ_Z) between $V_{\rm EMF}$ and $V_{\rm rec}$ explained in [22], and the phase difference (φ_{pf}) between $I_{\rm ref}$ and $V_{\rm EMF}$ caused by the *pf*. In Fig. 4, part B (or part D) consists of φ_Z and φ_{pf}, and their lengths increase. This means that the current can be more distorted by the open-circuit fault of the outer switches compared to when φ_Z alone is considered. Case I can be ignored because φ_Z is determined depending on the operating condition of the rectifier and the PMSG. However, because φ_{pf} is determined by the *pf*, Case II should be considered when the IPMSG is employed.

The current distortion caused by the open-circuit fault of the outer switches is shown in Fig. 5 for various *pfs*. Owing to the infeasible open-circuit fault switch, the current becomes zero during the range consisting of φ_Z and φ_{pf}. The S_{x1} open-circuit fault makes the current path of Fig. 2(d) infeasible. The current path of Fig. 2(d) belongs to part B; therefore, the S_{x1} open-circuit fault causes distortion in the negative current as shown in Fig. 5(a) and (c). On the contrary, the S_{x4} open-circuit fault leads to distortion in the positive current as shown in Fig. 5(b) and (d) because the current path of Fig. 2(c) related to the S_{x4} open-circuit fault belongs to part D.

The low *pf* has a large φ_{pf}. Therefore, the rectifier operation at a low *pf* leads to a large zero-current range when the open-circuit fault of the outer switch occurs. As a result, the zero-current range increases, as the *pf* decreases.

The analysis related to the open-circuit fault of the outer switches can be applied to the T-type topology. The effects of open-circuit faults of the outer switches on the current are the same in both the NPC rectifier and the T-type rectifier [13], [22]. Therefore, the current distortion caused by open-circuit faults of the outer switches in the NPC rectifier is the same as that in the T-type rectifier.

III. Tolerant Control for Open-Circuit Fault of Outer Switches

An existing tolerant control method for the open-circuit fault of the outer switches is reactive current injection [22]. This method changes the phase of $I_{\rm rec}$ so that it corresponds with the phase of $V_{\rm rec}$. This means that parts B and D are eliminated. However, this tolerant control method has the disadvantage of low-power generation efficiency of the generator because the PMSG has efficient operating condition which depends on the *pf* of the rectifier. In general, the unity *pf* is required for the best operating condition of a surface PMSG. The best operating condition of an IPMSG does not correspond to the unity *pf*, and this is determined by the specifications of the IPMSG.

The proposed tolerant control does not change the *pf* of the rectifier. The rectifier voltage ($V_{\rm rec}$) without the current path related to the open-circuit fault switch is generated by changing the reference voltages. To explain the proposed tolerant control, the S_{x1} open-circuit fault is used as an example.

A. Compensation Voltage ($V_{\rm comp}$) Calculation

Three-phase reference voltages ($V_{x,\rm ref}$, $x = a, b, c$) are expressed as

$$\begin{aligned} V_{a,\rm ref} &= V_{\rm mag}\cos(2\pi f_s t) \\ V_{b,\rm ref} &= V_{\rm mag}\cos(2\pi f_s t - 2\pi/3) \\ V_{c,\rm ref} &= V_{\rm mag}\cos(2\pi f_s t + 2\pi/3), \end{aligned} \tag{1}$$

where $V_{\rm mag}$ is the magnitude of the reference voltages, and f_s is the fundamental frequency.

The offset voltage ($V_{\rm offset}$) is added to each reference voltage to expand the range of the modulation index ($M_a = \sqrt{3} \times V_{\rm mag}/V_{\rm dc}$). $V_{\rm offset}$ and the changed reference voltages ($V_{x,\rm ref,offset}$, $x = a, b, c$) are expressed as

$$V_{\rm offset} = -(V_{\rm ref,max} + V_{\rm ref,min})/2, \tag{2}$$

$$\begin{aligned} V_{a,\rm ref,offset} &= V_{a,\rm ref} + V_{\rm offset} \\ V_{b,\rm ref,offset} &= V_{b,\rm ref} + V_{\rm offset} \\ V_{c,\rm ref,offset} &= V_{b,\rm ref} + V_{\rm offset} \end{aligned} \tag{3}$$

where $V_{\rm ref,max}$ and $V_{\rm ref,min}$ are the maximum and minimum values of $V_{a,\rm ref}$, $V_{b,\rm ref}$, and $V_{c,\rm ref}$. The reference voltages of (3) are compared with the carrier signals to generate $V_{\rm rec}$.

When the S_{x1} open-circuit fault occurs, the current path of Fig. 2(d) should be eliminated to prevent current distortion; therefore, the reference voltage should be changed to generate $V_{\rm rec}$ without the current path of Fig. 2(d). In the proposed tolerant control, a reference voltage of a phase containing the S_{x1} open-circuit fault is changed to zero as shown in Fig. 6. As a result, the current path of Fig. 2(d) disappears because the O switching state is only used in part B. To make the reference voltage zero, $|V_{\rm comp}|$ is assigned the magnitude of the reference voltage ($V_{x,\rm ref,offset}$) containing the open-circuit fault, and $V_{\rm comp}$ can be expressed as

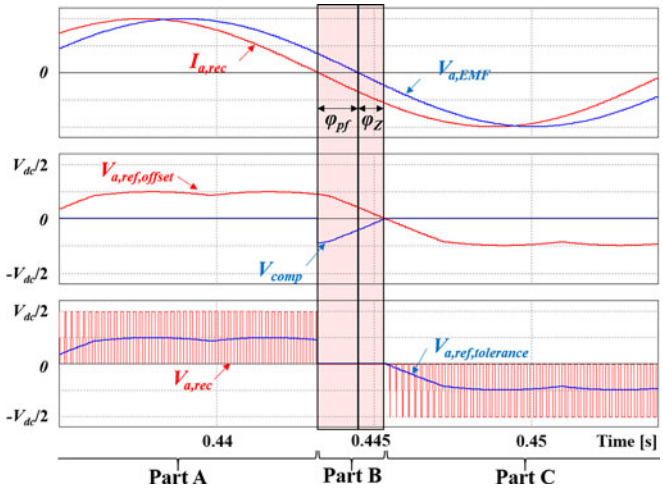

Fig. 6. Change of reference voltages in the proposed tolerant control for the S_{x1} open-circuit fault (0.95 *pf*).

$$V_{\rm comp} = -V_{\rm x,ref,offset}(x = \text{a phase containing open} - \text{circuited fault switch}). \tag{4}$$

The proposed tolerant control is implemented by adding $V_{\rm comp}$ to the reference voltages ($V_{x,\rm ref,offset}$, $x = a, b, c$). The new reference voltages ($V_{x,\rm ref,tolerance}$, $x = a, b, c$) of the proposed tolerant control are expressed as

$$\begin{aligned} V_{a,\rm ref,tolerance} &= V_{a,\rm ref,offset} + V_{\rm comp} \\ V_{b,\rm ref,tolerance} &= V_{b,\rm ref,offset} + V_{\rm comp} \\ V_{c,\rm ref,tolerance} &= V_{b,\rm ref,offset} + V_{\rm comp}. \end{aligned} \tag{5}$$

B. Compensation Range for Adding $V_{\rm comp}$

By adding $V_{\rm comp}$ to each reference voltage, the use of the current path related to the open-circuit fault switch will be precluded. To achieve this perfectly, $V_{\rm comp}$ is added for the suitable range and position. The compensation range, which is part B or part D of Fig. 4, consists of φ_Z and φ_{pf}. φ_Z can be calculated with the equivalent circuit of the PMSG and the three-level rectifier [22]. φ_Z, which is the phase difference between $V_{\rm EMF}$ and $V_{\rm rec}$, is expressed as

$$\varphi_Z = \tan^{-1}\left(\frac{-|I_{\rm rec}| \times 2\pi f_s L}{V_{\rm EMF} - |I_{\rm ref}|\, R}\right) \tag{6}$$

where *R* and *L* are the equivalent resistance and inductance of the PMSG, and f_s is the fundamental frequency representing the angular frequency of the PMSG.

φ_{pf}, which is the phase difference between $V_{\rm EMF}$ and $I_{\rm rec}$, is related to the *pf*. φ_{pf} can be calculated by the *pf* and this is

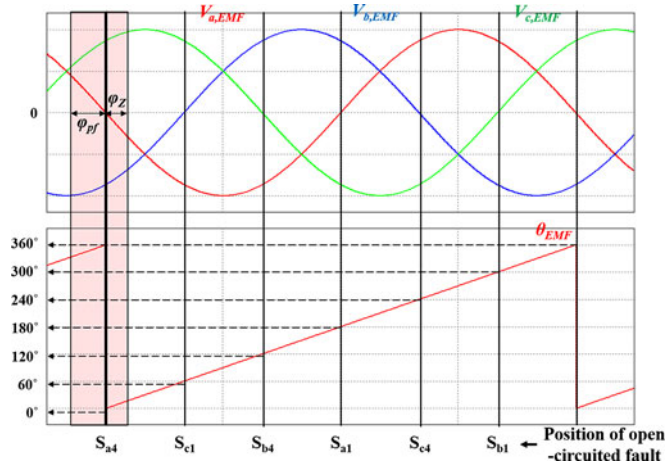

Fig. 7. Compensation position on the basis of V_{EMF}'s angle (θ_{EMF}).

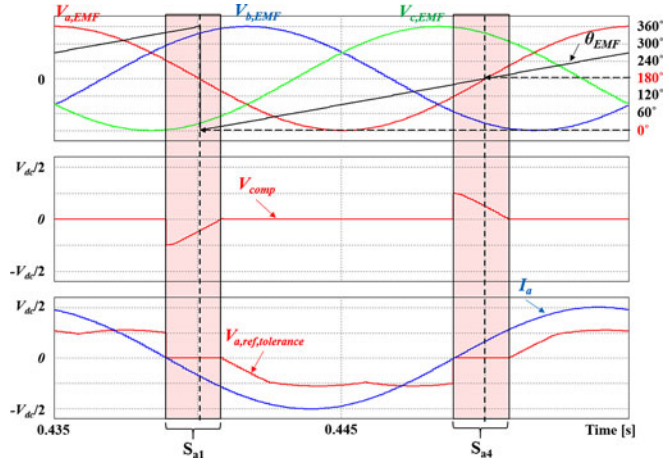

Fig. 8. Proposed tolerant control considering neutral-point voltage balance under the S_{a1} open-circuit fault.

TABLE II
COMPENSATION RANGE DEPENDING ON THE POSITION OF THE OPEN-CIRCUIT FAULT

Position of open-circuit fault	Compensation range
S_{a1}	$(0^\circ - \varphi_{pf}) \sim (0^\circ + \varphi_Z)$
S_{c4}	$(60^\circ - \varphi_{pf}) \sim (60^\circ + \varphi_Z)$
S_{b1}	$(120^\circ - \varphi_{pf}) \sim (120^\circ + \varphi_Z)$
S_{a4}	$(180^\circ - \varphi_{pf}) \sim (180^\circ + \varphi_Z)$
S_{c1}	$(240^\circ - \varphi_{pf}) \sim (240^\circ + \varphi_Z)$
S_{b4}	$(300^\circ - \varphi_{pf}) \sim (300^\circ + \varphi_Z)$

TABLE III
PRINCIPLE OF THE PROPOSED TOLERANT CONTROL DEPENDING ON THE POSITION OF THE OPEN-CIRCUIT FAULT

Position of open-circuit fault	V_{comp}	Compensation range
S_{a1} or S_{a4}	$-V_{a,\mathrm{ref,offset}}$	$(0^\circ - \varphi_{pf}) \sim (0^\circ + \varphi_Z)$
S_{c4} or S_{c1}	$-V_{c,\mathrm{ref,offset}}$	$(60^\circ - \varphi_{pf}) \sim (60^\circ + \varphi_Z)$
S_{b1} or S_{b4}	$-V_{b,\mathrm{ref,offset}}$	$(120^\circ - \varphi_{pf}) \sim (120^\circ + \varphi_Z)$
S_{a4} or S_{a1}	$-V_{a,\mathrm{ref,offset}}$	$(180^\circ - \varphi_{pf}) \sim (180^\circ + \varphi_Z)$
S_{c1} or S_{c4}	$-V_{c,\mathrm{ref,offset}}$	$(240^\circ - \varphi_{pf}) \sim (240^\circ + \varphi_Z)$
S_{b4} or S_{b1}	$-V_{b,\mathrm{ref,offset}}$	$(300^\circ - \varphi_{pf}) \sim (300^\circ + \varphi_Z)$

expressed as

$$\varphi_{pf} = \cos^{-1}(pf). \tag{7}$$

If the d–q control theorem is used, φ_{pf} can be calculated as

$$\varphi_{pf} = \cos^{-1}\left(\frac{I_{qe}}{\sqrt{I_{qe}^2 + I_{de}^2}}\right), \tag{8}$$

where I_{de} indicates the d-axis current related to the flux and I_{qe} indicates the q-axis current related to the torque, and these are values in the d–q synchronous rotating frame.

φ_Z and φ_{pf}, which are calculated from (6) and (8), are located near the zero-crossing point of V_{EMF} as shown in Fig. 6. Therefore, the compensation position for adding V_{comp} is defined on the basis of V_{EMF}'s angle (θ_{EMF}). Fig. 7 shows three-phase $V_{\mathrm{EMF}}s$ and θ_{EMF}. θ_{EMF} is acquired from the encoder or position sensor. Six zero-crossing points are expressed for every 60°, which are matched to each open-circuit fault as shown in Fig. 7. Consequently, θ_{EMF} representing each zero-crossing point is a criterion for adding V_{comp}. For example, when the S_{a1} open-circuit fault occurs, V_{comp} should be added for the compensation range from $(0^\circ - \varphi_{pf})$ to $(0^\circ + \varphi_Z)$ which is based on 0°. By considering all open-circuit faults, Table II shows the compensation ranges for eliminating the current distortion depending on the position of the open-circuit fault.

C. Considering Neutral-Point Voltage Balance

The compensation voltage which is one of the offset voltages can cause neutral-point voltage unbalance because V_{comp} calculated from (4) is a one-sided voltage [10], [24]. Therefore, two dc-link capacitors have different values depending on the polarity of V_{comp} generated for the open-circuit fault. The neutral-point voltage unbalance increases the voltage stress on the switch and the current THD [24].

The proposed tolerant control for the open-circuit fault of the outer switches has to incorporate a solution for the neutral-point voltage unbalance problem. Therefore, as mentioned earlier, V_{comp} is added for the corresponding compensation position depending on the position of the open-circuit fault, and then, V_{comp} is also added in the diametrically opposite compensation position to balance the neutral-point voltage. Fig. 8 shows the concept of proposed tolerant control considering the neutral-point voltage balance when the S_{a1} open-circuit fault occurs. In Fig. 8, V_{comp} is added for the compensation range $[(0^\circ - \varphi_{pf}) \sim (0^\circ + \varphi_Z)]$ which corresponds to the position for the S_{a1} open-circuit fault; in addition, V_{comp} is also added for the diametrically opposite compensation range $[(180^\circ - \varphi_{pf}) \sim (180^\circ + \varphi_Z)]$, which is the range for the S_{a4} open-circuit fault. Two V_{comp}s added in two positions have opposite polarity, and this results in the balanced neutral-point voltage.

The final principles of the proposed tolerant control with the neutral-point voltage balance are summarized in Table III.

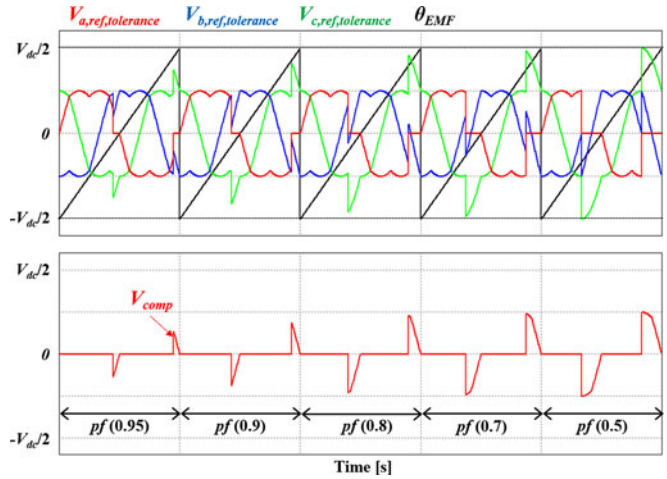

Fig. 9. $V_{x,\mathrm{ref,tolerance}}$ (x = a,b,c) and V_{comp} depending on the *pf* when M_a is 0.5.

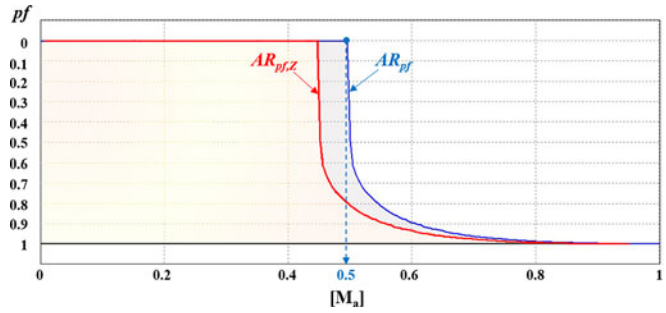

Fig. 10. Applicable *pf* range of the proposed tolerant control depending on M_a.

D. Limitation of Proposed Tolerant Control

$V_{x,\mathrm{ref,tolerance}}$ cannot exceed a limitation voltage (V_{limit}), which is restricted by the dc-link voltage (V_{dc}). Therefore, V_{comp} is limited as follows:

$$V_{\mathrm{comp}} < V_{\mathrm{limit}} - V_{\mathrm{ref,max}} \tag{9}$$

where V_{limit} is $V_{\mathrm{dc}}/2$.

On the basis of (9), the applicable operation range of the proposed tolerant control is determined depending on M_a and the *pf*. Fig. 9 shows $V_{x,\mathrm{ref,tolerance}}$ and V_{comp} of the proposed tolerant control depending on the *pf* when M_{a} is 0.5. In Fig. 9, V_{comp} leads to $V_{a,\mathrm{ref,tolerance}}$ with zero value in the corresponding compensation range. Moreover, the peak value of $V_{c,\mathrm{ref,tolerance}}$ increases owing to V_{comp}. As the *pf* decreases, this peak value increases; however, it does not exceed V_{limit}. Consequently, when M_a is smaller than 0.5, V_{comp} can be added regardless of the *pf* because $V_{c,\mathrm{ref,tolerance}}$ cannot exceed V_{limit}. When M_a is larger than 0.5, the applicable *pf* range is determined by M_a. This is because a low M_a provides a large margin for V_{comp}; however, a large V_{comp} cannot be acceptable for high M_a.

Fig. 10 shows the applicable *pf* range for various values of M_a. The shaded part of Fig. 10 represents the applicable operation range. The proposed tolerant control is feasible over the entire factor range when M_a is smaller than 0.5. By increasing M_a from 0.5, the applicable operation range decreases. In Fig. 10,

TABLE IV
IPMSG PARAMETERS IN SIMULATION

Rated power	2.5 MW
Number of pole	8
Rated voltage (line-to-line)	760 V_{rms}
Rated current	1902 A_{rms}
Rated speed	1650 rpm
Resistance	0.4567 mΩ
q-inductance	0.0982 mH
d-inductance	0.0725 mH

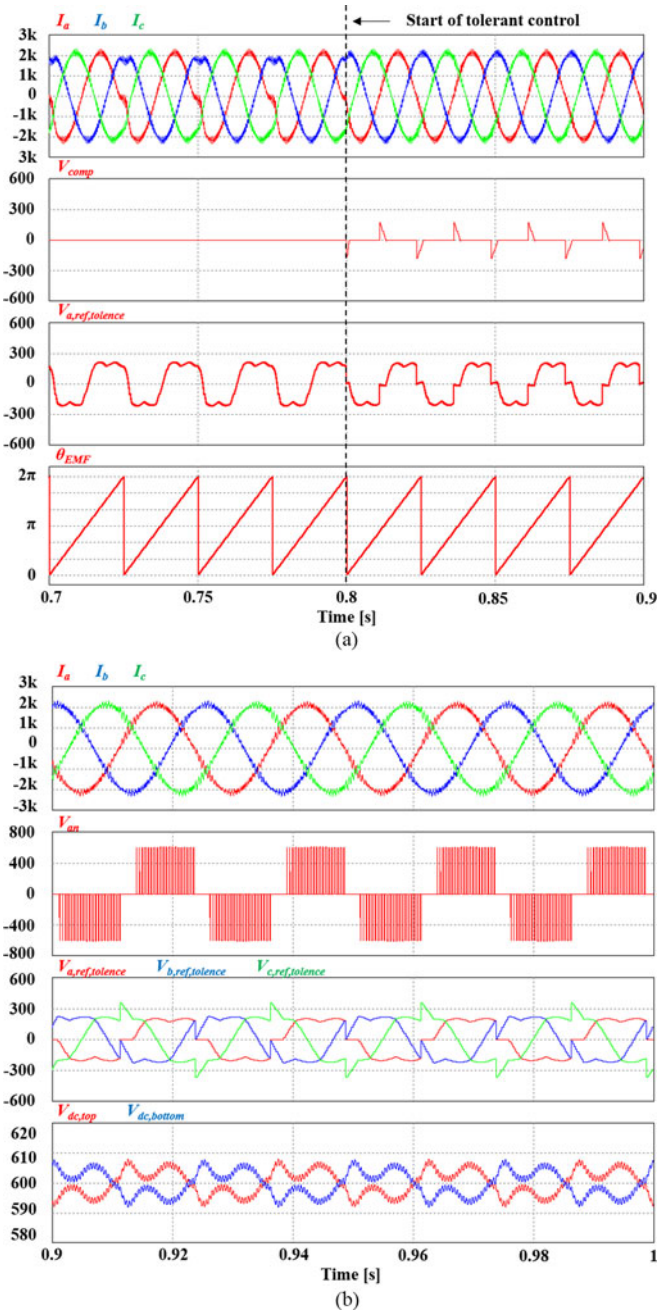

Fig. 11. Simulation results with the proposed tolerant control under the S_{a1} open-circuit fault (600 rpm, $M_a = 0.35, 0.95$ *pf*).

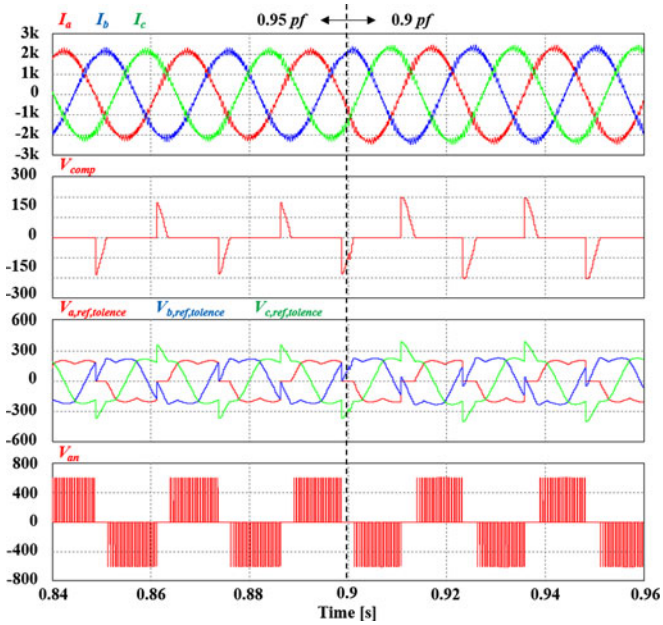

Fig. 12. Simulation results with the proposed tolerant control under the S_{a1} open-circuit fault (600 rpm, $M_a = 0.35$, *pf*-transition from 0.95 to 0.9).

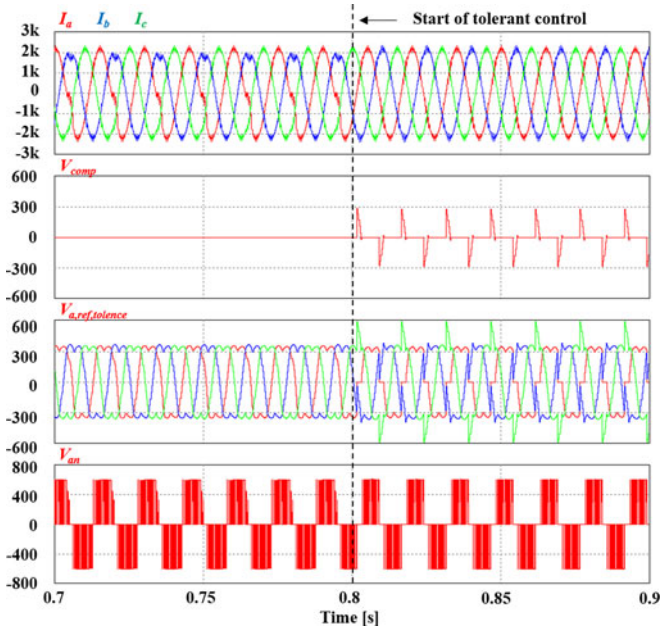

Fig. 13. Simulation results with the proposed tolerant control under the S_{a1} open-circuit fault (1000 rpm, $M_a = 0.59$, 0.95 *pf*).

TABLE V
CURRENT THD AND RMS VALUES COMPARISON (600 RPM, 0.95 *pf*)

	Normal (p.u.)	S_{a1} open-circuit fault	The proposed tolerant control
a-	$5.4\%, 1.51\,\mathrm{kA_{rms}}$	$14.8\%, 1.49\,\mathrm{kA_{rms}}$	$6.1\%, 1.51\,\mathrm{kA_{rms}}$
b-	$5.4\%, 1.51\,\mathrm{kA_{rms}}$	$9.4\%, 1.47\,\mathrm{kA_{rms}}$	$5.5\%, 1.51\,\mathrm{kA_{rms}}$
c-	$5.4\%, 1.51\,\mathrm{kA_{rms}}$	$8.1\%, 1.55\,\mathrm{kA_{rms}}$	$6.0\%, 1.51\,\mathrm{kA_{rms}}$

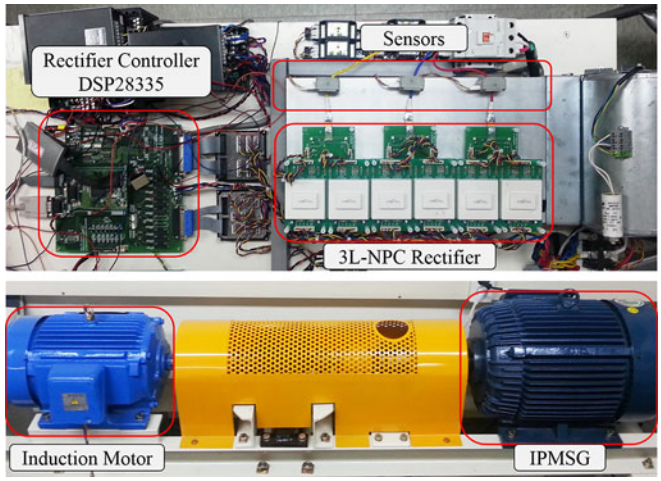

Fig. 14. Experimental setup of the 3L-NPC rectifier and the M–G set.

TABLE VI
IPMSG PARAMETERS IN THE EXPERIMENT

Rated power	11 kW
Number of pole	6
Rated voltage (line-to-line)	$380\,V_{\mathrm{rms}}$
Rated current	$19.9\,A_{\mathrm{rms}}$
Rated speed	1750 rpm
Resistance	0.349 Ω
q-inductance	15.6 mH
d-inductance	13.16 mH

the applicable operation range shown as AR_{pf} is largest when only the *pf* related to φ_{pf} is taken into account. However, a large φ_Z means that large portion of the compensation range is reserved for φ_Z, and the rest can be used to compensate φ_{pf}. Therefore, φ_Z caused by the impedance of the PMSG reduces the applicable *pf* range, and it is shown in $AR_{\mathrm{pf,Z}}$ with $\varphi_Z = 10$. φ_Z is determined by the operation conditions and parameters of the PMSG shown in (6).

The proposed tolerant control has a limitation on its operation range that depends on the *pf* and M_a. However, considering that wind turbine systems do not always operate with the rated wind speed (high M_a) and that the operating *pf* of the rectifier with an IPMSG is not too low, the proposed tolerant control can clearly be effective.

IV. SIMULATION RESULTS

The simulation is performed using the PSIM tool. The 3L-NPC rectifier of the back-to-back converter with 2.5-MW IPMSG is only considered in the simulation. The simulation parameters are as follows: the switching frequency is 2 kHz, the control period is 250 μs, the dc-link capacitor is 35 mF, and the dc-link voltage is 1200 V. The IPMSG parameters used in the simulation are shown in Table IV. The proposed tolerant control for the open-circuit fault of the outer switches (S_{x1}, S_{x4}) is implemented for different *pfs* and generator speeds.

Fig. 11 shows the simulation results of the proposed tolerant control when the $\mathrm{S_{a1}}$ open-circuit fault occurs. The speed

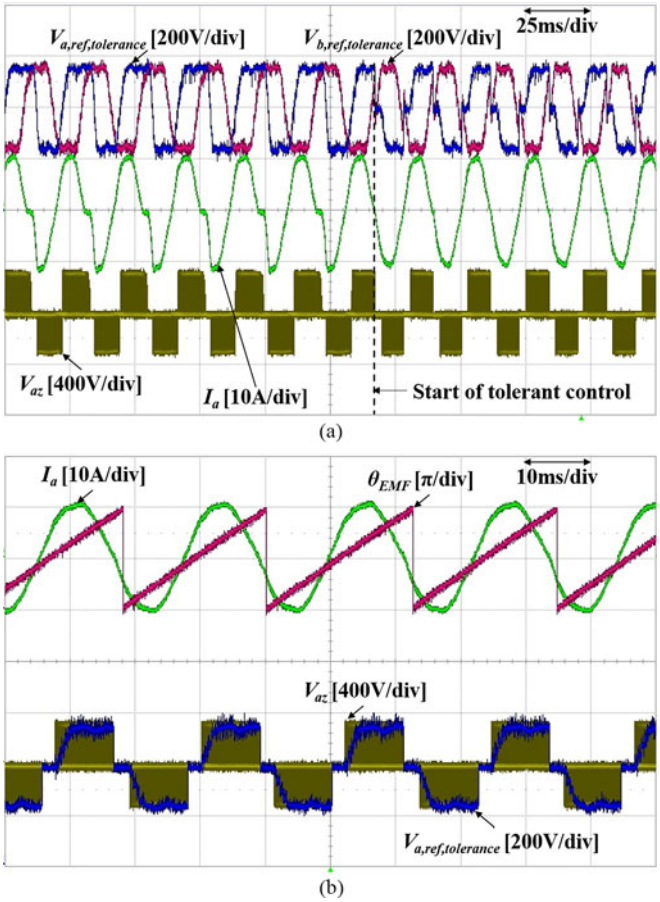

Fig. 15. Experimental results with the proposed tolerant control under the S_{a1} open-circuit fault (900 rpm, $M_a = 0.5$, 0.95 *pf*).

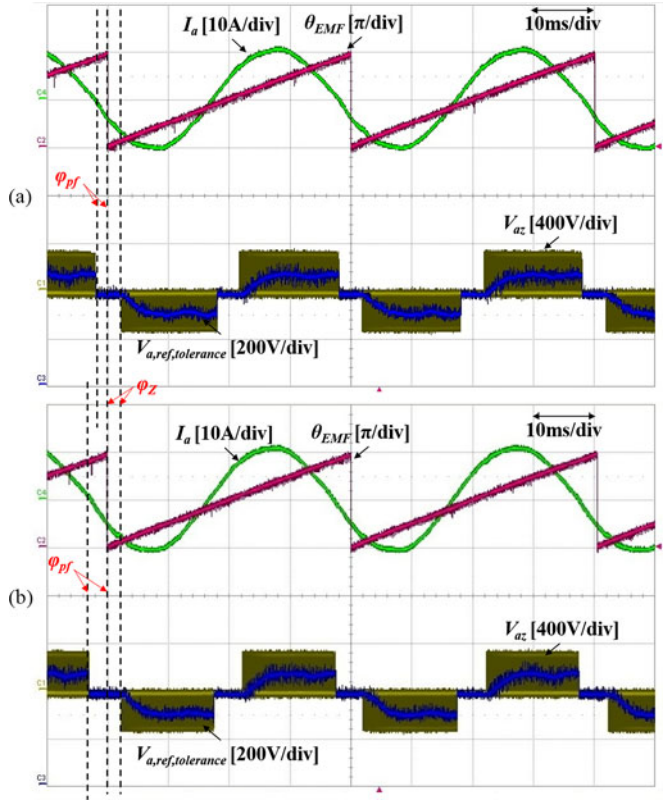

Fig. 16. Experimental results with the proposed tolerant control at different *pfs* (450 rpm, $M_a = 0.25$): (a) 0.95 *pf* and (b) 0.9 *pf*.

of the PMSG is 600 rpm, M_a is 0.35, and the *pf* of the rectifier is 0.95. Owing to the S_{a1} open-circuit fault, the negative current is distorted as shown in Fig. 11(a). After the proposed tolerant control is applied, the reference voltages are changed by $V_{\rm comp}$ for the corresponding ranges $[(0^\circ - \varphi_{pf}) \sim (0^\circ + \varphi_Z), (180^\circ - \varphi_{pf}) \sim (180^\circ + \varphi_Z)]$ which are defined in Table III. As a result, the a-phase pole voltage (V_{an}) is clamped to 0 at their ranges as shown in Fig. 11(b) and the current distortion is eliminated completely. In addition, the two dc-link capacitor voltages are balanced.

The proposed tolerant control is effective for the *pf* transition operation of the rectifier. Fig. 12 shows the results when the proposed tolerant control is applied and the *pf* is changed from 0.95 to 0.9. The compensation range is extended as much as the *pf* decreases and the currents are maintained without distortion continuously. Moreover, we know that the peak value of $V_{c,{\rm ref,tolerance}}$ becomes large because the *pf* decreases which was discussed in Section III.

Fig. 13 shows the performance of the proposed tolerant control under the S_{a1} open-circuit fault at different speed (1000 rpm) of the PMSG when M_a is 0.59. Similar to Fig. 11, the distorted currents are corrected after the proposed tolerant control is applied. However, the peak value of $V_{c,{\rm ref,tolerance}}$ is close to $V_{\rm limit}(V_{\rm dc}/2)$ at 0.95 *pf*, which is different from what is shown in Fig. 11. This is because $M_{\rm a}$ of Fig. 13 has a smaller applicable operation range than that of Fig. 11, which can be seen in Fig. 10.

Table V shows the current THD results before and after the proposed tolerant control is applied. The current THD is increased by the S_{a1} open-circuit fault; however, owing to the proposed tolerant control, the current THD is restored as good as normal state without any open-circuit fault.

V. Experimental Results

Experiments are conducted to identify the performance of the proposed tolerant control for open-circuit faults of the outer switches. In Fig. 14, the low-power prototype hardware setup consists of the power converter and the M–G set. The induction motor operates as the blade of wind turbine systems; therefore, the gear box is not used in the experiment. In addition, the 3L-NPC insulated gate bipolar transistor modules (Semikron, SK75MLI066T) are used in the experiment. The experimental setup parameters are as follows: the switching frequency is 10 kHz, the control period is 100 μs, the dc-link capacitor is 1100 μF, and the dc-link voltage is 600 V. The IPMSG parameters used in the experiment are shown in Table VI.

Fig. 15 shows the performance of the proposed tolerant control when the S_{a1} open-circuit fault occurs. The speed of the PMSG is 900 rpm, M_a is 0.5, and the *pf* is 0.95. Similar to the simulation results, the S_{a1} open-circuit fault causes current distortion, as shown in Fig. 15(a). After the proposed tolerant control is applied, the reference voltages are changed

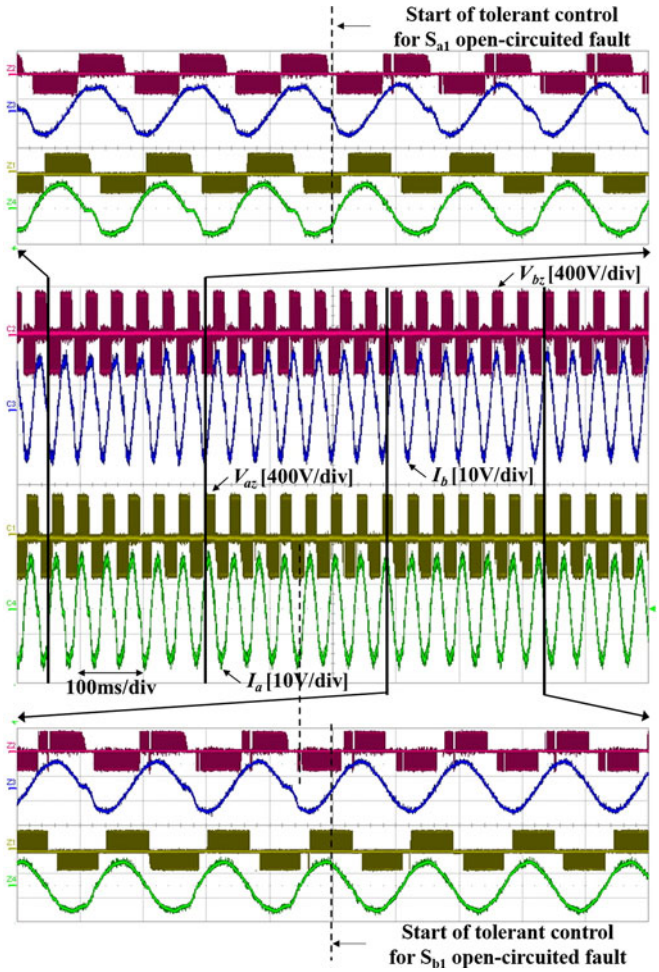

Fig. 17. Experimental results with the proposed tolerant control under the S_{a1} and S_{b1} open-circuit faults (450 rpm, $M_a = 0.25, 0.95$ *pf*).

by $V_{\rm comp}.V_{\rm comp}$ is added for the corresponding compensation ranges with the S_{a1} open-circuit fault defined in Table III as shown in Fig. 15(b). The a-phase pole voltage (V_{an}) is zero for these ranges; therefore, the current path related to the S_{a1} open-circuit fault is not used, and current distortion is eliminated.

Fig. 16 shows the compensation range of the proposed tolerant control for different *pfs*. As the *pf* decreases, the compensation range is extended. Closer inspection reveals that the *pf* is only related to φ_{pf}; therefore, φ_Z is almost unchanged in Fig. 16(a) and (b).

The proposed tolerant control can respond to open-circuit faults of two switches. In Fig. 17, S_{a1} and S_{b1} open-circuit faults occur, and the proposed tolerant control for each fault is applied in order. First, the tolerant control for the S_{a1} open-circuit fault is applied and the distorted a-phase current (I_a) is corrected. Second, the b-phase current (I_b) distortion caused by the S_{b1} open-circuit fault is also eliminated.

VI. Conclusion

This paper proposes a tolerant control for the open-circuit fault of the outer switches in three-level rectifiers (both 3L-NPC and T-type topologies) used in wind turbine systems. The reason why the tolerant control for the open-circuit fault of the outer switches in three-level rectifiers is necessary is presented, together with the supporting circuit analysis. On the basis of the analysis, a tolerant control for each open-circuit fault is proposed that takes into account the neutral-point voltage balance. This control is implemented by adding a compensation voltage ($V_{\rm comp}$) to the reference voltages for the corresponding compensation ranges depending on the position of the open-circuit fault. Furthermore, this control can be used in both the 3L-NPC and T-type rectifiers and guarantees normal operation without a change of the *pf* in the applicable operation range shown in Fig. 10 depending on the modulation index (M_a) and the *pf*. Although the operating range of the proposed tolerant control is subject to a limitation, considering that wind turbine systems do not always operate with the rated wind speed and that the operating *pf* of the rectifier with an IPMSG is not too low, the proposed tolerant control is clearly effective. The performance and effectiveness of the proposed tolerance control are proved through simulations and experiments.

References

[1] A. Isidori, F. M. Rossi, F. Blaabjerg, and K. Ma, "Thermal loading and reliability of 10-MW multilevel wind power converter at different wind roughness classes," *IEEE Trans. Ind. Appl.*, vol. 50, no. 1, pp. 484–494, Jan./Feb. 2014.

[2] H. G. Jeong, K. B. Lee, S. Chio, and W. Choi, "Performance improvement of LCL-filter-based grid-connected inverters using PQR power transformation," *IEEE Trans. Power Electron.*, vol. 25, no. 5, pp. 1320–1330, May 2010.

[3] S. Li, T. A. Haskew, R. P. Swatloski, and W. Gathings, "Optimal and direct-current vector control of direct-driven PMSG wind turbines," *IEEE Trans. Power Electron.*, vol. 27, no. 5, pp. 2325–2337, May 2012.

[4] W. Qiao, L. Qu, and R. G. Harley, "Control of IPM synchronous generator for maximum wind power generation considering magnetic saturation," *IEEE Trans. Ind. Appl.*, vol. 45, no. 3, pp. 1095–1105, May/Jun. 2009.

[5] S. Morimoto, H. Nakayama, M. Sanada, and Y. Takeda, "Sensorless output maximization control for variable-speed wind generation system using IPMSG," *IEEE Trans. Ind. Appl.*, vol. 41, no. 1, pp. 60–67, Jan./Feb. 2005.

[6] Y. Zhao, W. Qiao, and L. Wu, "An adaptive quasi-sliding-mode rotor position observer-based sensorless control for interior permanent magnet synchronous machines," *IEEE Trans. Power Electron.*, vol. 28, no. 12, pp. 5618–5629, Dec. 2013.

[7] P. B. Reddy, A. M. EL-Refaie, and K. K. Huh, "Effect of number of layers on performance of fractional-slot concentrated-windings interior permanent magnet machines," *IEEE Trans. Power Electron.*, vol. 30, no. 4, pp. 2205–2218, Apr. 2015.

[8] J. S. Lee and K. B. Lee, "New modulation techniques for a leakage current reduction and a neutral-point voltage balance in transformerless photovoltaic systems using a three-level inverter," *IEEE Trans. Power Electron.*, vol. 29, no. 4, pp. 1720–1732, Apr. 2014.

[9] U. M. Choi, H. G. Jeong, K. B. Lee, and F. Blaabjerg, "Method for detecting an open-switch fault in a grid-connected NPC inverter system," *IEEE Trans. Power Electron.*, vol. 27, no. 6, pp. 2726–2739, Jun. 2012.

[10] U. M. Choi, J. S. Lee, and K. B. Lee, "New modulation strategy to balance the neutral-point voltage for three-level neutral-clamped inverter systems," *IEEE Trans. Energy Convers.*, vol. 29, no. 1, pp. 91–100, Mar. 2014.

[11] M. Schweizer and J. W. Kolar, "Design and implementation of a highly efficient three-level t-type converter for low-voltage applications," *IEEE Trans. Power Electron.*, vol. 28, no. 2, pp. 899–907, Feb. 2013.

[12] U. M. Choi, F. Blaabjerg, and K. B. Lee, "Reliability improvement of a t-type three-level inverter with fault-tolerant control strategy," *IEEE Trans. Power Electron.*, vol. 30, no. 5, pp. 2660–2673, May 2015.

[13] J. S. Lee and K. B. Lee, "An open-switch fault detection method and tolerance controls based on SVM in a grid-connected t-type rectifier with unity power factor," *IEEE Trans. Ind. Electron.*, vol. 61, no. 12, pp. 7092–7104, Dec. 2014.

[14] H. K. Ku, W. S. Im, J. M. Kim, and Y. S. Suh, "Fault detection and tolerant control of 3-phase NPC active rectifier," in *Proc. IEEE Energy Convers. Congr. Expo.*, Sep. 2012, pp. 4519–1524.
[15] J. S. Lee, K. B. Lee, and F. Blaabjerg "Open-switch fault detection method of an NPC converter for wind turbine systems," in *Proc. IEEE Energy Convers. Congr. Expo.*, Sep. 2013, pp. 1696–1701.
[16] S. Ceballos, J. Pou, E. Robles, J. Zaragoza, and J. L. Martín, "Performance evaluation of fault-tolerant neutral-point-clamped converters," *IEEE Trans. Ind. Electron.*, vol. 57, no. 8, pp. 2709–2718, Aug. 2010.
[17] J. Li, A. Q. Huang, Z. Liang, "Analysis and design of active NPC (ANPC) inverters for fault-tolerant operation of high-power electrical drives," *IEEE Trans. Power Electron.*, vol. 27, no. 2, pp. 519–533, Feb. 2012.
[18] Y. Song and B. Wang, "Survey on reliability of power electronic systems," *IEEE Trans. Power Electron.*, vol. 28, no. 1, pp. 591–604, Jan. 2013.
[19] S. Li and L. Xu, "Strategies of fault tolerant operation for three-level PWM inverters," *IEEE Trans. Power Electron.*, vol. 21, no. 4, pp. 933–940, Jul. 2006.
[20] J. S. Lee, U. M. Choi, and K. B. Lee, "Comparison of tolerance controls for open-switch fault in a grid-connected T-type rectifier," *IEEE Trans. Power Electron.*, vol. 30, no. 10, pp. 5810–5820, Nov. 2014.
[21] U. M. Choi, F. Blaabjerg, and K. B. Lee, "Reliability improvement of a T-type three-level inverter with fault-tolerant control strategy," *IEEE Trans. Power Electron.*, vol. 30, no. 5, pp. 2660–2673, May 2015.
[22] J. S. Lee and K. B. Lee, "Open-switch fault tolerance control for a three-level NPC/T-type rectifier in wind turbine systems," *IEEE Trans. Ind. Electron.*, vol. 62, no. 2, pp. 1012–1021, Feb. 2015.
[23] J. S. Lee, K. B. Lee, and F. Blaabjerg, "Open-switch fault detection method of a back-to-back converter using NPC topology for wind turbine systems," *IEEE Trans. Ind. Appl.*, vol. 51, no. 1, pp. 325–335, Jan./Feb. 2015.
[24] Y. Jiao, F. C. Lee, and S. Lu, "Space vector modulation for three-level NPC converter with neutral point voltage balance and switching loss reduction," *IEEE Trans. Power Electron.*, vol. 29, no. 10, pp. 5579–5591, Oct. 2014.

June-Seok Lee (S'11) received the B.S. and M.S. degrees in electrical and computer engineering from Ajou University, Suwon, Korea, in 2011 and 2013, respectively, where he is currently working toward the Ph.D. degree.

His research interests include grid-connected systems, multilevel inverter, and reliability.

Kyo-Beum Lee (S'02–M'04–SM'10) received the B.S. and M.S. degrees in electrical and electronic engineering from Ajou University, Suwon, Korea, in 1997 and 1999, respectively. He received the Ph.D. degree in electrical engineering from Korea University, Seoul, Korea, in 2003.

From 2003 to 2006, he was with the Institute of Energy Technology, Aalborg University, Aalborg, Denmark. From 2006 to 2007, he was with the Division of Electronics and Information Engineering, Chonbuk National University, Jeonju, Korea. In 2007, he joined the School of Electrical and Computer Engineering, Ajou University, Suwon, Korea. His research interests include electric machine drives, renewable power generations, and electric vehicle applications.

Dr. Lee is an Associate Editor of the IEEE TRANSACTIONS ON POWER ELECTRONICS, the *Journal of Power Electronics*, and the *Journal of Electrical Engineering and Technology*.